RRB-87-48

UTILIZING THE COMPONENTS OF VECTOR IRRADIANCE TO ESTIMATE THE SCALAR IRRADIANCE IN NATURAL WATERS

by

J.H. Jerome, R.P. Bukata,
and J.E. Bruton

Rivers Research Branch
National Water Research Institute
Canada Centre for Inland Waters
Burlington, Ontario, Canada L7R 4A6

NWRI Contribution #87-148

ABSTRACT

A Monte Carlo computer simulation has been used to determine the ratio of the scalar irradiance (E_0) to the downwelling irradiance (E_d). These E_0/E_d ratios were calculated at depths corresponding to the 100%, 10% and 1% downwelling irradiance levels. A range of volume reflectance $0 \leq R \leq 0.14$ was considered, as were six conditions of incident radiation (collimated beams with incident angles $0 \leq \theta' \leq 89°$, plus diffusive cardioidal). Mathematical expressions were curve-fitted to the Monte Carlo outputs to yield relationships between E_0/E_d and R for the depths and incident conditions considered. It was found that in many instances a single relationship would not accommodate the entire range of volume reflectances and that R=0.055 provided an appropriate demarcation for mathematical curve fitting. Curves, tables, and equations are presented which indicate a) for all $R > \sim 0.02$, the E_0/E_d ratio at the 1% downwelling irradiance depth is the same for $\theta' = 0°$ as for diffusive cardioidal incidence, b) for $R > \sim 0.08$, the E_0/E_d ratio at the 10% downwelling irradiance depth for $\theta' = 0°$ is nearly the same as the E_0/E_d ratio at the 1% downwelling irradiance depth for diffusive cardioidal incidence, and c) the scalar irradiance may be confidently determined from direct measurement of downwelling and upwelling irradiances.

RÉSUMÉ

Un programme de simulation informatique Monte Carlo a été utilisé afin de déterminer l'éclairement énergétique scalaire (E_0) par rapport à l'éclairement énergétique de la descente des eaux (E_d). Ces rapports E_0/E_d ont été calculés à des profondeurs correspondant à des taux d'éclairement énergétique de descente des eaux de 100 %, 10 % et 1 %. On a pris en considération une plage de réflectances volumétriques de $0 \leq R \leq 0.14$ ainsi que six conditions de rayonnement incident (faisceaux collimatés ayant des angles incidents de $0 \leq \theta' \leq 89°$, plus un cardioïde de diffusion). Des expressions mathématiques ont été ajustées aux courbes des résultats du programme Monte Carlo pour générer des équations établissant des rapports entre E_0/E_d et R pour les profondeurs et les conditions incidentes considérées. On a trouvé que dans bien des cas, une simple équation ne tient pas compte de toute la plage de réflectances volumétriques et que R = 0,055 constituait une démarcation appropriée pour un ajustement mathématique des courbes. Des courbes, des tableaux et des équations sont présentés et indiquent que: a) pour tous les R sup. à env. 0,02, le rapport E_0/E_d à la profondeur d'un éclairement énergétique de descente des eaux de 1 % est le même pour $\theta = 0°$ que pour l'incidence cardioïdale de diffusion, b) pour les R sup. à env. 0.08, le rapport E_0/E_d à une profondeur d'éclairement énergétique de descente des eaux de 10 % pour $\theta' = 0°$ est presque le même que le rapport E_0/E_d à la profondeur d'éclairement énergétique de descente des eaux de 1 % pour l'incidence cardioïdale de diffusion, et c) l'éclairement énergétique scalaire peut être déterminé de façon sûre grâce à la mesure directe des éclairements éngergétiques de descente et de montée des eaux.

MANAGEMENT PERSPECTIVE

The fact that natural light is one of the main controlling parameters of both the biological and chemical configurations of natural water masses is indisputable. Equally indisputable is the need to accurately ascertain the amount of light, as a function of depth, which is available in the subsurface environment for photochemical activities, whether the optical target be an algal cell or a photo-degradable contaminant. Traditionally, direct measurements of optical flux profiles have concentrated on upwelling and downwelling irradiances. These valuable and reliable parameters certainly contribute substantially to the basic understanding of inland water behaviour. However, since upwelling and downwelling irradiances are vector quantities, they are, understandably, strongly influenced by the directional properties of the above-surface incident energy (photon) distribution. Consequently, the appropriateness of such vector parameters to monitor the energy to which a biological cell or contaminant is exposed, is somewhat suspect. The scalar irradiance, however, is a measure of the total energy at a point in the water column when all directions have been equally weighted. The appropriateness of such an energy monitor to evaluate photochemistry is subject to considerably less suspicion.

This manuscript develops a model for utilizing the readily-determinable and reliable measurements of upwelling and downwelling irradiance profiles to estimate the less-readily-determinable (and hitherto overly-ignored) scalar irradiance. Computer simulations of subsurface photon propagation using Monte Carlo techniques are used to

arrive at the mathematical relationships uniting the vector quantities with the scalar quantity. While there is certainly a considerable amount of work yet to be performed, this model represents an essential first step in accurately estimating the amount of light available for photochemical activity.

PERSPECTIVE - GESTION

Le fait que la lumière naturelle soit l'un des principaux paramètres de contrôle des configurations biologiques et chimiques des masses d'eau naturelle est incontestable. La nécessité de vérifier avec précision, en fonction de la profondeur, la quantité de lumière disponible dans un milieu sous-marin pour les activités photochimiques, que la cible optique soit une cellule d'algues ou un contaminant photodégradable, est également indéniable. Les mesures directes des profils de flux optique ont toujours été basées sur l'éclairement énergétique de la montée et de la descente des eaux. Ces paramètres importants et fiables contribuent certainement de façon importante à la compréhension fondamentale du comportement des eaux intérieures. Cependant, étant donné que les taux d'éclairement énergétique de la montée et de la descente des eaux sont des quantités vectorielles, ceux-ci sont naturellement fortement influencées par les propriétés directionnelles de la distribution de l'énergie incidente (photons) au-dessus de la surface. Par conséquent, l'utilité de ces vecteurs pour vérifier le plux d'énergie auquel une cellule biologique ou un contaminant est exposé est quelque peu douteuse. L'éclairement énergétique ou un contaminant est exposé est quelque peu douteuse. L'éclairement énergétique scalaire est cependant une mesure de l'énergie totale à un point donné dans la colonne d'eau lorsque toutes les directions ont été pondérées de façon adéquate. Une telle mesure de l'énergie convient donc beaucoup mieux pour évaluer l'énergie photochimique.

Le présent manuscrit élabore un modèle d'utilisation de mesures fiables, faciles à déterminer, de profils d'éclairement énergétique de la montée et de la descente de l'eau, pour évaluer l'éclairement énergétique scalaire moins facile à établir (et donc longtemps ignoré). Les simulations par ordinateur de la propagation des photons sous la surface de l'eau à l'aide des techniques de Monte Carlo sont utilisées pour obtenir les équations mathématiques qui intègrent les quantités vectorielles à la quantité scalaire. Ce modèle représente une première étape essentielle dans l'estimation précise de la quantité de lumière disponible pour l'activité photochimique, bien qu'il reste encore beaucoup de travail à faire dans ce domaine.

INTRODUCTION

The subsurface downwelling and upwelling irradiances (the components of the vector irradiance) have long been the commonly measured in situ quantities in optical studies of natural water masses. The popularity of such optical properties is due, in no small part, to the relative ease encountered in their measurement, and the availability of reliable instrumentation with which to perform such measurements. However, since the subsurface downwelling and upwelling irradiances are vector quantities, their measured magnitudes are strongly influenced by the directions of the incident photons, and, consequently, they are not the most appropriate parameters for monitoring the energy to which an algal cell or photo-degradable contaminant is exposed.

The scalar irradiance is the total energy per unit area arriving at a point from all directions when all directions are equally weighted. Thus, when divided by the speed of light in water, the scalar irradiance yields the radiant energy density, i.e. the radiant energy per unit volume at a point within the water column. The appropriateness of utilizing scalar irradiance measurements to monitor the available energy for photosynthesis has long been advocated (Atkins and Poole[1,2]).

This communication presents the results of employing Monte Carlo simulations of photon propagation through natural water columns to determine the functional relationships among upwelling and downwelling irradiances (i.e. components of the vector irradiance) and the scalar irradiance.

METHODOLOGY

A fixed scattering to absorption ratio (b/a) and a fixed scattering phase function ($\beta(\theta)$) were supplied as inputs to the Monte Carlo simulation of photon propagation. The water column was assumed to be homogeneous. For a given incident light distribution the photons were tracked and recorded to give the scalar irradiance levels, E_0 at the depths of the 100%, 10% and 1% downwelling irradiance levels, E_d. That is, the scalar irradiance E_0 was determined for depths Z_{100}, Z_{10} and Z_1 corresponding to the depths of the downwelling irradiance levels of 100%, 10%, and 1%, respectively. In addition, the Monte Carlo simulation was used to determine the upwelling irradiance E_u at Z_{100} (i.e. just beneath the air/water interface).

From these values, the ratios E_0/E_d were readily determined at Z_{100}, Z_{10} and Z_1, as was the volume reflectance $R = E_u/E_d$ at Z_{100} (i.e. R just below the surface. This value of R at Z_{100} is the variable considered in all subsequent equations in this manuscript.)

To illustrate that the appropriate choice in independent variable for defining the quantity E_0/E_d is the volume reflectance, R, (proportional to Bb/a where B is the backscattering probability) rather than the scattering to absorption ratio b/a, the Monte Carlo simulation was utilized for a single fixed value of b/a and three scattering phase functions (Petzold[3]) with backscattering probabilities B=0.013, 0.025, and 0.044. This resulted in three distinct values of E_0/E_d for the single value of b/a. These three

values of E_o/E_d, however, were linearly related to Bb/a, indicating, in agreement with the work of Prieur and Sathyendranath[4] that the ratio E_o/E_d is a function of the volume reflectance R. Thus, for the purpose of this work, the volume reflectance was considered as the controlling parameter, and its value was varied by ascribing a fixed value of B (in this analysis B = 0.025) to a set of b/a values which included b/a = 1, 3, 5, 8, 10, 12, and 18. Six conditions of incident radiation were considered, corresponding to collimated beams with incident zenith angles θ' of 0°, 30°, 45°, 60°, and 89°, as well as a diffusive cardioidal incident distribution.

ANALYSES

a) For Z_{100} (i.e. the 100% downwelling irradiance depth)

Figure 1 illustrates the value of E_o/E_d resulting from the Monte Carlo simulation for collimated vertical incidence (θ' = 0°) and Z_{100} as a function of volume reflectance R (R is also taken as the value appropriate to Z_{100} and θ' = 0°. A method for obtaining this R from a volume reflectance associated with a non-vertical incident radiation field is given by Jerome et al[5].) The least squares fit to the values of Figure 1 yields:

$$\frac{E_o}{E_d}(R,0°) = 1 + 3.13\,R \qquad (1)$$

with a coefficient of variation $r^2 = 0.99$.

Prieur and Sathyendranath[4] express the E_o/E_d ratio as:

$$\frac{E_o}{E_d}(R) = \frac{1}{\bar{\mu}_d} + \frac{R}{\bar{\mu}_u} \qquad (2)$$

where $\bar{\mu}_d$ and $\bar{\mu}_u$ are the mean cosines for the downwelling and upwelling irradiance fields, respectively.

Comparing equations (1) and (2) would suggest that $1/\bar{\mu}_d = 1.0$ and $1/\bar{\mu}_u = 3.13$. For the diverse radiant fields and depths considered by Prieur and Sathyendranath[4], the values of $1/\bar{\mu}_u$ varied from 2.3 to 3.0. This places the $1/\bar{\mu}_u$ value suggested by equation (1) just outside this range. This is a consequence of $1/\bar{\mu}_d$ not being exactly equal to 1.0 for vertical incidence due to internal reflections of the upwelling irradiance. Since the amount of total internally reflected energy will increase with increasing R, this departure of $\bar{\mu}_d$ from a value of 1.0 (corresponding to the condition of vertical incidence with no volume reflectance) is incorporated into the constant 3.13. Consequently, it must be emphasized that the two terms on the right hand side of equation (1) are not directly comparable to the two terms on the right hand side of equation (2).

Figure 2 displays the dependence of the E_o/E_d ratio on the directionality of the incident radiation field. Herein is plotted the ratio of the value of E_o/E_d for a given angle θ' to its value for vertical incidence (i.e. $\theta' = 0°$) as a function of $1/\mu_o$ (the inverse of the cosine of the in-water angle of refraction θ_o). The plotted ordinate value for each of the five incident angles of Figure 2 is the average of the ordinate values for each of the seven volume reflectance values considered in this work.

The linear relationship of Figure 2 is given by:

$$\frac{E_o}{E_d}(R,\theta') = \left[\frac{1.068}{\mu_o} - 0.068\right]\frac{E_o}{E_d}(R,0°) \qquad (3)$$

with $r^2 = 0.99$.

The slope of Figure 2, being greater than 1, indicates that the value of E_o/E_d as a function of R and θ' increases with increasing θ_o at a rate greater than that which would result from the cosine effect alone. Reiterating, this is likely attributable to total internal reflection.

Figure 3 illustrates the total internal reflection ρ_{INT} experienced by the upwelling subsurface irradiance plotted as a function of $1/\mu_o$. The relationship of Figure 3, which emerged from the Monte Carlo simulation, may be expressed as

$$\rho_{INT} = \frac{0.249}{\mu_o} + 0.271 \qquad (4)$$

with $r^2 = 0.98$.

For the condition of vertical incidence ($\mu_o = 1$) equation (4) yields a value of $\rho_{INT} = 0.520$ which may be compared to the value of 0.485 obtained by Gordon[6] assuming a diffuse upwelling field.

Thus, for a given volume reflectance R, the total internal reflection ρ_{INT} increases with increasing incidence angle θ', contributing to the slope >1 of Figure 2.

Combining equations (1) and (3) the ratio E_o/E_d at Z_{∞} is given by:

$$\frac{E_o}{E_d}(R,\theta') = \left[\frac{1.068}{\mu_o} - 0.068 \right] \left[1 + 3.13\, R \right] \qquad (5)$$

It is understood in equation (5) that while the θ' values may vary between 0° and 89°, the R values are constrained to the value for $\theta' = 0°$. Figure 4 illustrates the E_o/E_d versus R curves resulting from equation (5) for $Z_{1\infty}$ and angles $\theta' = 0°$, 30°, 45°, 60°, and 89° (reading from bottom to top, respectively). For comparison, the values resulting from the Monte Carlo simulation program are shown as points. The average magnitude of the differences between the Monte Carlo and equation (5) outputs is ~0.5%.

b) For Z_{10} (i.e. the 10% downwelling irradiance depth)

At the depth of the 10% downwelling irradiance level (Z_{10}) it was observed that the variation in E_o/E_d with R and μ_o was similar to that reported by Kirk[7] for the change in K_d/a with b/a and μ_o (where K_d is the downwelling vertical irradiance attenuation coefficient and all other terms are as previously defined). Therefore, it was assumed that an appropriate equation relating E_o/E_d (at Z_{10}) to R would be of the form:

$$\frac{E_o}{E_d}(R, \theta') = \frac{1}{\mu_o} \left[1 + (C_1 \mu + C_2 R + C_3)\, R \right]^{C_4} \qquad (6)$$

where C_1, C_2, C_3, and C_4 are constants, and R is the volume reflectance value for $Z_{1\infty}$ and $\theta' = 0°$.

Equation (6) appropriately reduces to $E_o/E_d = 1/\mu_o$ in the absence of volume reflectance (i.e. for the condition of b = 0).

However, great difficulty was encountered when attempting to fit equation (6) to the outputs of the Monte Carlo simulation as a single continuous curve over the entire range of R considered herein, strongly suggestive of the need to consider curve-fitting to limited ranges of volume reflectance.

Further, it was noted that for a given R, changes in E_o/E_d varied linearly with $1/\mu_o$. It was deemed appropriate, therefore, to curve-fit (segmentally in R) the E_o/E_d versus R form of equation (6) for the enveloping θ' conditions of $\theta' = 0°$ and $\theta' = 89°$, and interpolate for the intermediate values of θ'. The results of such curve fitting were as follows:

For the case of $\theta' = 0°$,

$$\frac{E_o}{E_d}\ (R, 0°) = [\ 1 + (28.0 - 50.5R)\ R\ ]^{0.5} \qquad (7)$$

for $0 \leq R \leq 0.14$, i.e. for the entire range of volume reflectance values considered by this work to logically represent that which would normally be observed in both inland lake and ocean waters for $\theta' = 0°$. Extrapolation of equation (7) beyond R = 0.14 would be considered tenuous.

For the case of $\theta' = 89°$ the volume reflectance range was considered to be appropriately divided into a non-linear range ($0 \leq R \leq 0.055$) and a linear range ($0.055 \leq R \leq 0.14$). Utilizing this demarcation of volume reflectance into a lower range R_L and a higher range R_H, the resulting pair of equations became:

$$\frac{E_o}{E_d}(R_L,89°) = 1.512\left[\,1 + (7.39 - 149R + 1376R^2)\,R\,\right]^{1.0} \qquad (8)$$

for $0 \leq R_L \leq 0.055$

and $$\frac{E_o}{E_d}(R_H,89°) = 1.60 + 3.43\,R \qquad (9)$$

for $0.055 \leq R_H \leq 0.14$.

As mentioned earlier, the estimation of E_o/E_d for values of θ' intermediate to 0° and 89° was accomplished by interpolation using a linear function of $1/\mu_o$.

Thus, for $0 \leq R_L \leq 0.055$,

$$\frac{E_o}{E_d}(R_L,\theta') = \frac{E_o}{E_d}(R_L,0°) + \left(\frac{\cos 48.6°}{1-\cos 48.6°}\right)\left(\frac{1-\mu_o}{\mu_o}\right)\left[\frac{E_o}{E_d}(R_L,89°) - \frac{E_o}{E_d}(R_L,0°)\right] \qquad (10)$$

In a similar manner interpolations between equations (7) and (9) may be established for the volume reflectance range $0.055 \leq R_H \leq 0.14$.

Figure 5 shows the curves resulting from the use of equations (7), (8), (9), and their interpolations (such as represented by equation (10)). Also shown are the (E_o/E_d, R) pairs resulting from the Monte Carlo simulation. The average magnitude of the differences between the curves and Monte Carlo points of Figure 5 is 0.7%, indicating an excellent agreement among the curve-fitting techniques and Monte Carlo analyses for $Z_{1,0}$.

c) For Z_1 (i.e. the 1% downwelling irradiance depth)

At the depth of the 1% downwelling irradiance level it was again deemed appropriate to segment the volume reflectance curve-fitting at R = 0.055. The equations resulting from the regression analyses for the lower range of volume reflectance values ($0 \leq R_L \leq 0.055$) were:

$$\frac{E_o}{E_d}(R_L,0°) = [\ 1 + (39.1 - 176R)\ R\ ]^{0.5} \qquad (11)$$

$$\frac{E_o}{E_d}(R_L,89°) = 1.512\ [\ 1 + (-2.10 + 117R - 582R^2)\ R\ ]^{0.8} \qquad (12)$$

$$\frac{E_o}{E_d}(R_L,\theta') = \frac{E_o}{E_d}(R_L,0°) + \left(\frac{\cos 48.6°}{1-\cos 48.6°}\right)\left(\frac{1-\mu_o}{\mu_o}\right)\left[\frac{E_o}{E_d}(R_L,89°) - \frac{E_o}{E_d}(R_L,0°)\right] \qquad (13)$$

For the higher range of volume reflectance values ($0.055 \leq R_H \leq 0.14$) it was found that for a given R_H the Monte Carlo simulation yielded E_o/E_d values (for the entire θ' interval) within such a narrow range that the statistical scatter resulted in the E_o/E_d values being interspersed independently of μ_o. Consequently, for $0.055 \leq R_H \leq 0.14$ a single linear relationship between E_o/E_d and R was considered in the curve-fitting activity, utilizing the average of the E_o/E_d values obtained by varying μ_o at a fixed value of R_H. For each of the four values of $R_H > 0.055$, the standard deviations as a consequence of varying θ' was about 0.04, while the range of E_o/E_d values using the full spectrum of θ' values was

only ±0.045 from the average E_0/E_d value. It would therefore appear that the incident angle has very little effect on the E_0/E_d ratio at the 1% downwelling irradiance depth (Z_1) for water masses characterized by volume reflectances $\geq$ 0.055.

As will be discussed more fully in the next section, the single linear equation for E_0/E_d at Z_1 for $0° \leq \theta' \leq 89°$ and $0.055 \leq R_H \leq 0.14$ which was curve-fitted as:

$$\frac{E_0}{E_d}(R_H,\theta') = 1.37 + 4.93\ R \qquad (14)$$

is, in actuality, the equivalent relationship appropriate to Z_1 and Z_{1_0} for the condition of diffusive cardioidal incident radiation.

Figure 6 illustrates the curves resulting from the use of equations (11), (12), and (14) and the interpolation (as represented by equation (13)). Also shown are the $(E_0/E_d,R)$ values resulting from the Monte Carlo simulation. The magnitude of the average difference between the equations and the Monte Carlo simulation is 1.4%

d) <u>For diffusive cardioidal incidence</u>

Employing a cardioidal distribution for the incident radiation field, the Monte Carlo simulation yielded a relationship between E_0/E_d and R at Z_{1_∞} of the form:

$$\frac{E_o}{E_d}(R) = 1.177\ [\ 1 + 3.13\ R\ ] \qquad (15)$$

which, by comparison to equation (1), can be seen to be 1.177 times the relationship appropriate for vertical incidence ($\theta' = 0°$).

Setting equation (15) ($Z_{1\infty}$ for cardioidal incidence) equal to equation (5) ($Z_{1\infty}$ for vertical incidence) and solving for μ_o, a value $\mu_o = 0.858$ is obtained which is in excellent agreement with the value of 0.859 given by Prieur and Sathyendranath[4] as the average in-water cosine value for a cardioidal distribution.

Further, the use of a cardioidal distribution for the incident radiation field resulted in the Monte Carlo simulation yielding E_o/E_d values for $Z_{1\infty}$ and Z_1 which were nearly equivalent for a given value of R.

Once again the segmentation of the volume reflectance regime into R_L and R_H at a value of 0.055 was strongly suggested by the Monte Carlo output, and for $0 \leq R_L \leq 0.055$ and diffusive cardioidal incidence, curve-fitting the Monte Carlo results at both $Z_{1\infty}$ and Z_1 yielded the relationship:

$$\frac{E_o}{E_d}(R_L) = 1.177\ [\ 1 + (11.8 + 96.8\ R)\ R\ ]^{0.5} \qquad (16)$$

Table I lists the E_o/E_d ratio values resulting from the Monte Carlo simulation for the four R_H values > 0.055 at the $Z_{1\infty}$ and Z_1 depths assuming a diffusive cardioidal incident radiation field.

Also, for comparison, Table I lists the average of the E_0/E_d ratios resulting from the Monte Carlo simulation for these R_H values at the Z_1 level assuming a series of collimated incident radiation fields with incident zenith angles of 0°, 30°, 45°, 60°, and 89°. Clearly, the three sets of numerical entries in Table I are very similar, further accentuating the minimal role played by the incident angle θ' in the numerical value of the E_0/E_d ratio at Z_1 for volume reflectances > 0.055.

It was therefore considered not inappropriate to represent all three sets of entries in Table I by the same linear relationship.

Thus, for $0.055 \leq R_H \leq 0.14$, for both depths Z_{10} and Z_1 and diffusive cardioidal incident radiation, as well as for depth Z_1 and collimated incident radiation, equation (14), as alluded to earlier, is considered a multi-duty relationship. The average magnitude of the differences between the E_0/E_d values emerging from equations (14), (15) and (16) and the Monte Carlo simulations for Z_{100}, Z_{10} and Z_1 and conditions of cardioidal incident distribution is ~0.8%.

DISCUSSION

Table II lists the values of the E_0/E_d ratio for vertical incidence at Z_{100}, Z_{10}, and Z_1 and for diffusive cardioidal incidence at Z_1. These parameters are listed as the numerical solutions from the E_0/E_d equations for several values of R. Also tabulated are the ratios of both Z_1 and Z_{10} for vertical incidence to Z_1 for

diffusive cardioidal incidence [i.e. $Z_1(0°)/Z_1(diff)$ and $Z_{1\circ}(0°)/Z_1(diff)$]. It is seen from Table II that:

a) The E_0/E_d ratio for vertical incidence at Z_1 is virtually equivalent to the E_0/E_d ratio for diffusive incidence at Z_1 for all volume reflectance values $R > \sim 2\%$.

b) The E_0/E_d ratio for vertical incidence at $Z_{1\circ}$ is numerically very close to the E_0/E_d ratio for diffusive incidence at Z_1 for volume reflectance values $R > \sim 2\%$. This is particularly true for volume reflectance values $R > \sim 8\%$ where the $Z_{1\circ}(0°)/Z_1(diff)$ ratios are 0.97.

Table II therefore suggests that at the 10% subsurface downwelling irradiance depth ($Z_{1\circ}$) the radiance distribution is not substantially different from the asymptotic radiance distribution for $R > \sim 8\%$. It may not be unreasonable, therefore, to further suggest that many of the relationships derived for conditions of asymptotic radiance distribution, while totally appropriate to depths as shallow as Z_1 for all values of $R > \sim 2\%$, may also be totally appropriate to more shallow depths ($Z_{1\circ}$) for all values of $R > \sim 8\%$.

Prieur and Sathyendranath[4] have derived an expression for defining the absorption coefficient a(Z) in terms of a number of parameters, one of the parameters being the ratio E_0/E_d. Each of these parameters, with the exception of E_0/E_d, is determinable from profiles of upwelling and downwelling irradiances. The E_0/E_d equations and graphical representations included within this communication afford the opportunity of also being able to determine

E_o/E_d from profiles of upwelling and downwelling irradiances. Thus, the methodology of Prieur and Sathyendranath[4] may be used to calculate a(Z) without the necessity of invoking approximating assumptions.

REFERENCES

1. W.R.G. Atkins and H.H. Poole, J. Marine Biol. Assoc. U.K. 24, 271 (1940).
2. W.R.G. Atkins and H.H. Poole, J. Int. Council Exploration Sea 23, 327 (1958).
3. T.J. Petzold, Volume Scattering Functions for Selected Waters (Scripps Institution of Oceanography, University of California at San Diego, 1972), SIO Ref. 72-78.
4. L. Prieur and S. Sathyendranath, Limnol. Oceanogr. 26, 671 (1981).
5. J.H. Jerome, R.P. Bukata and J.E. Bruton, Appl. Opt. (in press).
6. J.I. Gordon, Directional Radiance (Luminance) of the Sea Surface (Scripps Institution of Oceanography, University of California at San Diego, 1969), SIO Ref. 69-20.
7. J.T.O. Kirk, Limnol. Oceanogr. 29, 350 (1984).

TABLE I: Values of the ratio E_o/E_d for volume reflectances >0.055

Volume Reflectance R_H	E_o/E_d Ratio		
	Diffuse Incidence and Z_{1o}	Diffuse Incidence and Z_1	Average of Angular Incidence and Z_1
0.0640	1.670	1.701	1.708
0.0806	1.755	1.769	1.771
0.0937	1.858	1.870	1.859
0.1331	2.009	2.050	2.012

TABLE II: Values of the ratio E_0/E_d at various depths for conditions of vertical and diffusive incidence

Volume Reflectance	E_0/E_d Ratio				$\frac{Z_1(0°)}{Z_1(diff)}$	$\frac{Z_{10}(0°)}{Z_1(diff)}$
	$Z_{100}(0°)$ (vertical)	$Z_{10}(0°)$ (vertical)	$Z_1(0°)$ (vertical)	$Z_1(diff)$ (Diffusive)		
0.0078	1.024	1.102	1.138	1.233	0.92	0.89
0.0237	1.074	1.279	1.352	1.359	0.99	0.94
0.0406	1.127	1.433	1.516	1.507	1.01	0.95
0.0640	1.200	1.608	1.686	1.686	1.00	0.95
0.0806	1.252	1.711	1.767	1.767	1.00	0.97
0.0937	1.293	1.783	1.832	1.832	1.00	0.97
0.1331	1.417	1.958	2.026	2.026	1.00	0.97

FIGURE CAPTIONS

Figure 1: Relationship between the ratio E_o/E_d and volume reflectance for Z_{100} and vertical incidence.

Figure 2: The ratio E_o/E_d for Z_{100} and incident angle θ' to E_o/E_d for Z_{100} and vertical incidence plotted as a function of the inverse of the cosine θ_o.

Figure 3: The total internal reflection ρ_{INT} plotted as a function of the inverse of the cosine of θ_o.

Figure 4: E_o/E_d versus R curves fitted to Monte Carlo simulation outputs for Z_{100} and $\theta' = 0°$, $30°$, $45°$, $60°$, and $89°$.

Figure 5: E_o/E_d versus R curves fitted to Monte Carlo simulation outputs for Z_{10} and $\theta' = 0°$, $30°$, $45°$, $60°$, and $89°$.

Figure 6: E_o/E_d versus R curves fitted to Monte Carlo simulation outputs for Z_1 and $\theta' = 0°$, $30°$, $45°$, $60°$, and $89°$. For $R > 0.055$, the E_o/E_d values have been shown as the average values of the Monte Carlo outputs for all incident angles along with its standard deviation.

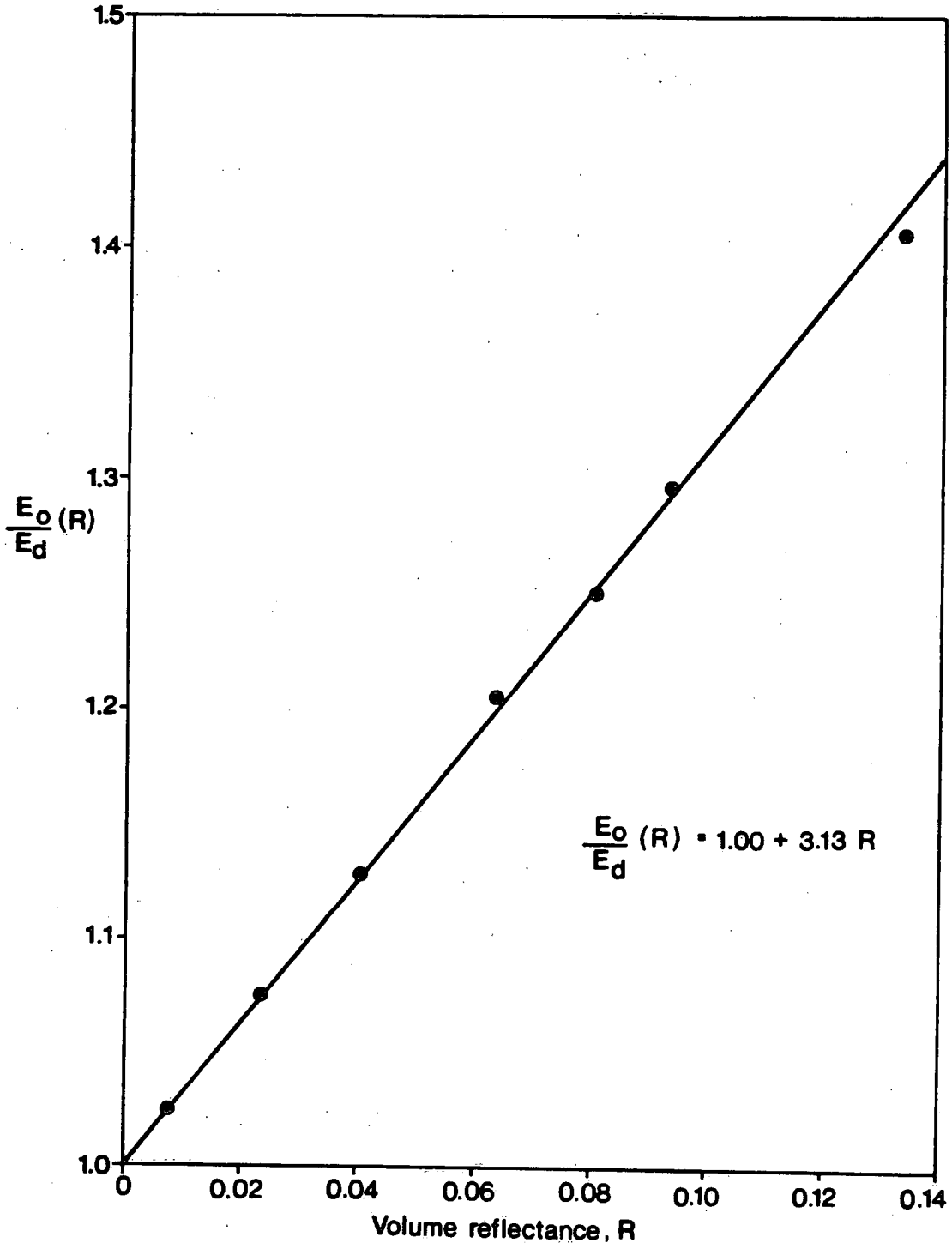
1.5
1.4
1.3
1.2
1.1
1.0
$\frac{E_o}{E_d}$ (R)
$\frac{E_o}{E_d}$ (R) = 1.00 + 3.13 R
0
0.02
0.04
0.06
0.08
0.10
0.12
0.14
Volume reflectance, R

FIGURE 1

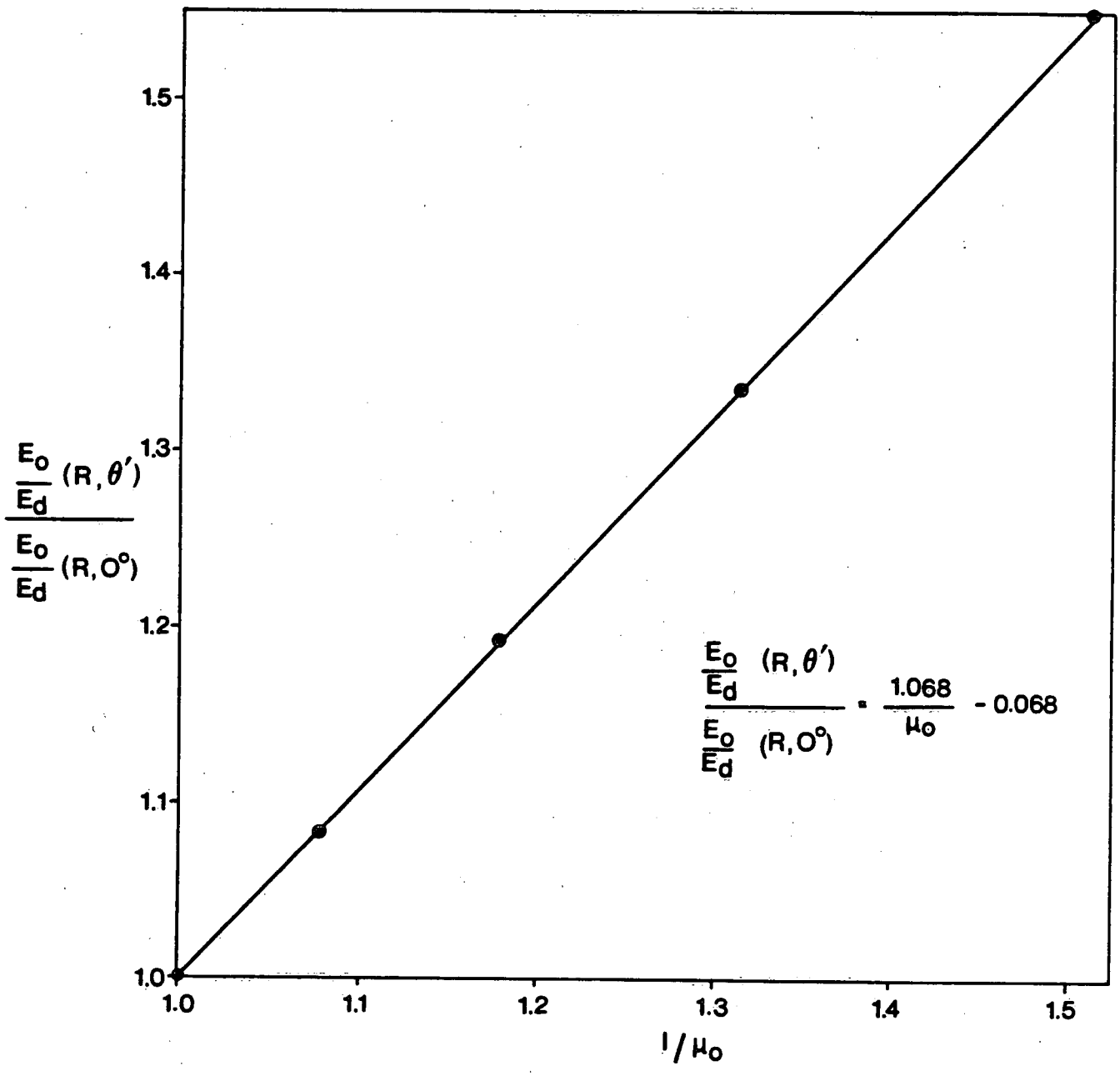
1.5
1.4
1.3
1.2
1.1
1.0
1.0
1.1
1.2
1.3
1.4
1.5
$\frac{E_o}{E_d}(R,\theta')$ / $\frac{E_o}{E_d}(R,0^\circ)$
$1/\mu_o$
$\frac{E_o}{E_d}(R,\theta') = \frac{1.068}{\mu_o} - 0.068$

FIGURE 2

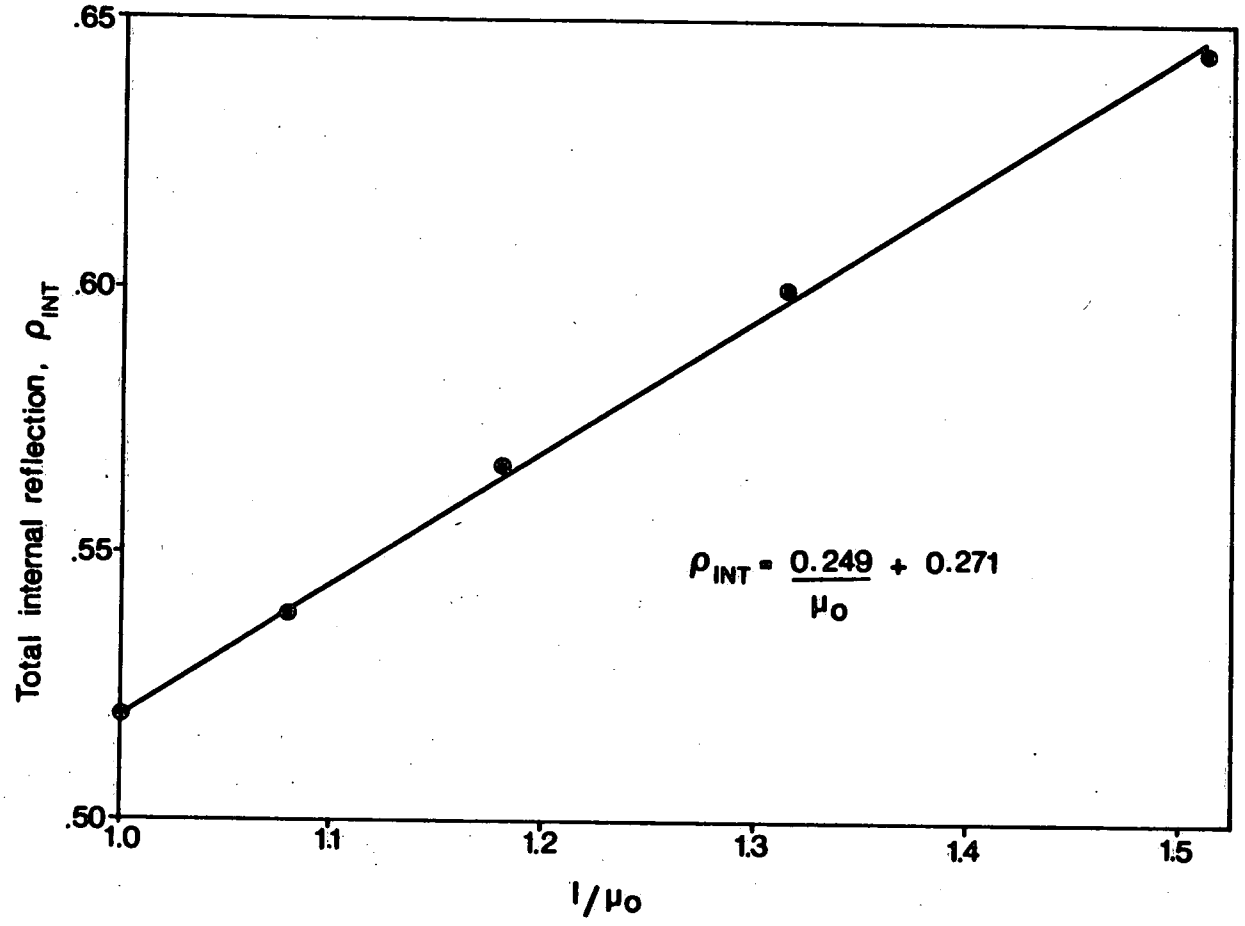
.65
.60
.55
.50
Total internal reflection, ρ_{INT}
$\rho_{INT} = \frac{0.249}{\mu_o} + 0.271$
1.0
1.1
1.2
1.3
1.4
1.5
$1/\mu_o$

FIGURE 3

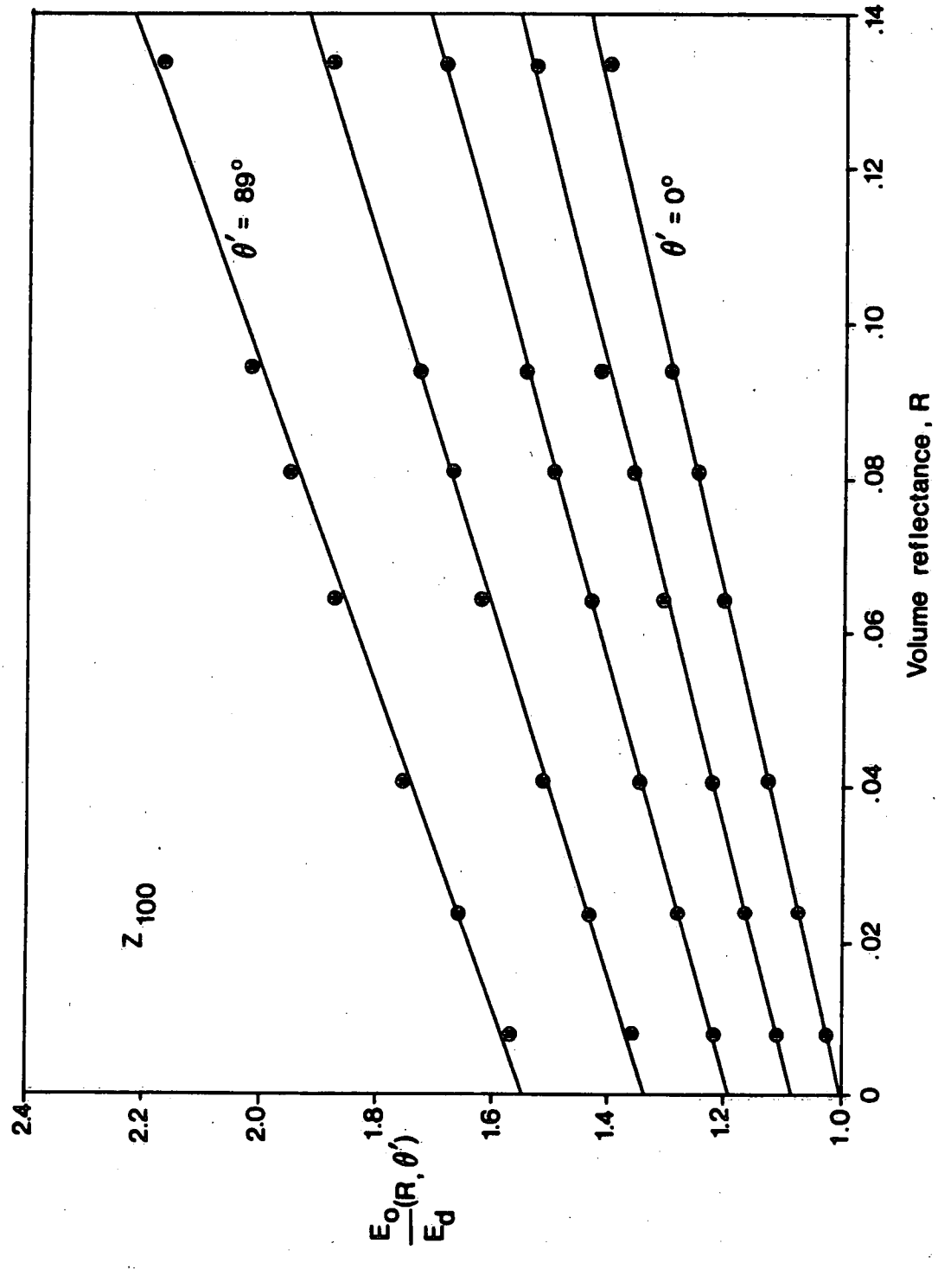
Z_{100}
$\theta' = 89°$
$\theta' = 0°$
$\frac{E_o}{E_d}(R, \theta')$
2.4
2.2
2.0
1.8
1.6
1.4
1.2
1.0
0
.02
.04
.06
.08
.10
.12
.14
Volume reflectance, R

FIGURE 4

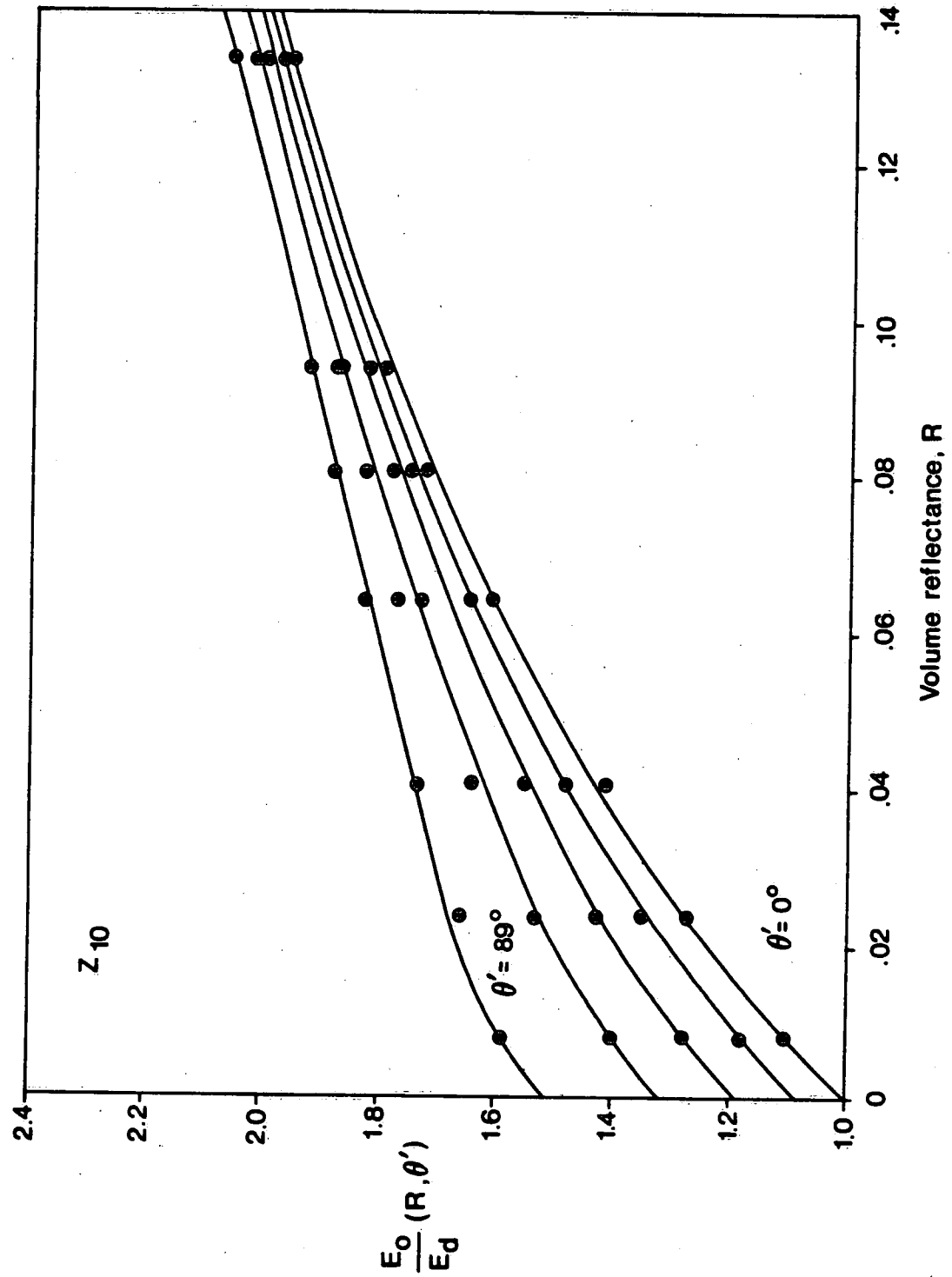
Z 10
θ'= 89°
θ'= 0°
$\frac{E_o}{E_d}(R,\theta')$
Volume reflectance, R
2.4
2.2
2.0
1.8
1.6
1.4
1.2
1.0
0
.02
.04
.06
.08
.10
.12
.14

FIGURE 5

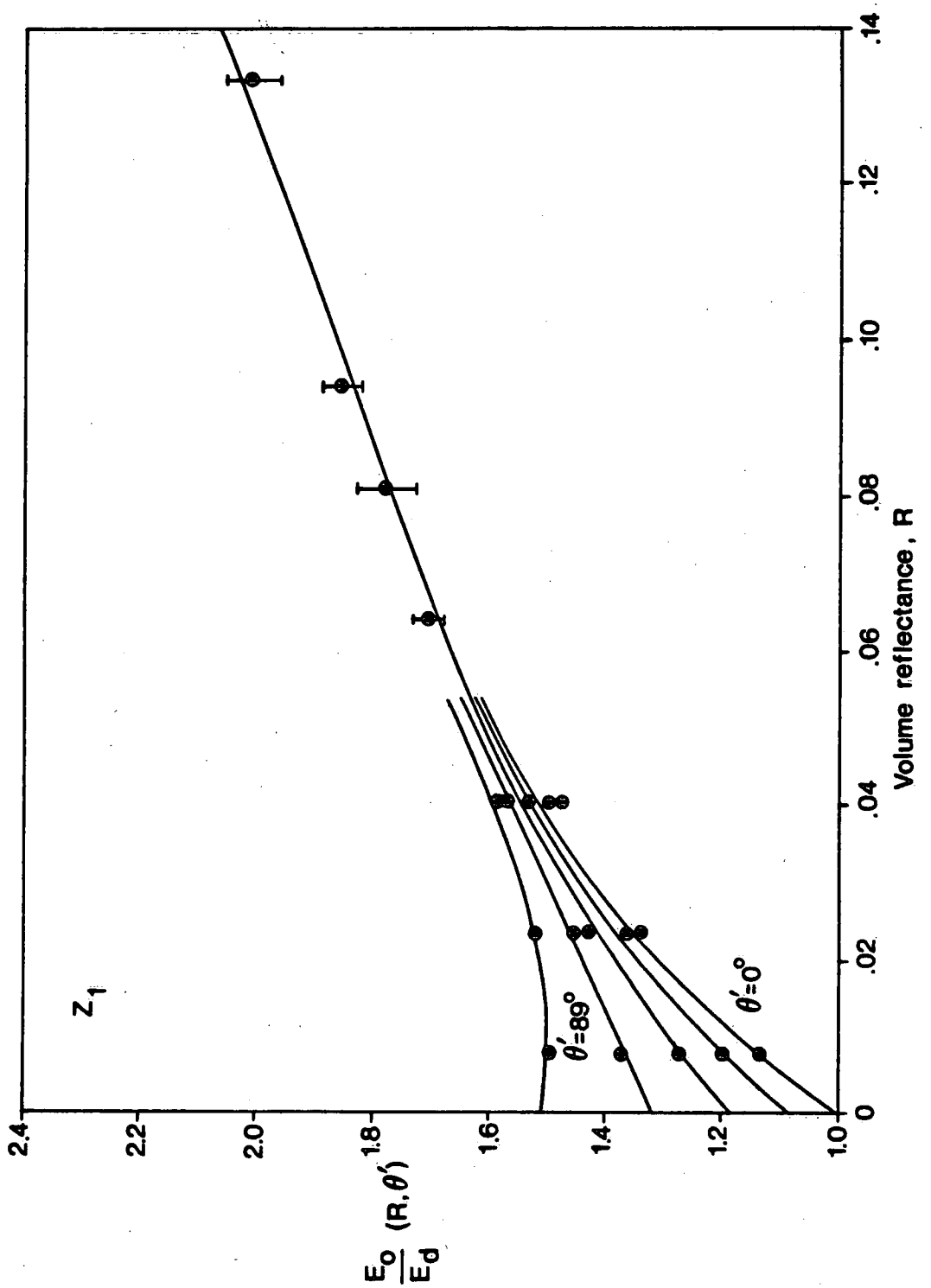
Z_1
θ'=89°
θ'=0°
$\frac{E_o}{E_d}$ (R, θ')
Volume reflectance, R
2.4
2.2
2.0
1.8
1.6
1.4
1.2
1.0
0
.02
.04
.06
.08
.10
.12
.14

FIGURE 6